

# Accounting for Optimal Control in the Sizing of Isolated Hybrid Renewable Energy Systems Using Imitation Learning

Simon Halvdansson<sup>1</sup>, Lucas Ferreira Bernardino<sup>1</sup>, Brage Rugstad Knudsen<sup>1</sup>

**Abstract**—Decarbonization of isolated or off-grid energy systems through phase-in of large shares of intermittent solar or wind generation requires co-installation of energy storage or continued use of existing fossil dispatchable power sources to balance supply and demand. The effective CO<sub>2</sub> emission reduction depends on the relative capacity of the energy storage and renewable sources, the stochasticity of the renewable generation, and the optimal control or dispatch of the isolated energy system. While the operations of the energy storage and dispatchable sources may impact the optimal sizing of the system, it is challenging to account for the effect of finite horizon, optimal control at the stage of system sizing. Here, we present a flexible and computationally efficient sizing framework for energy storage and renewable capacity in isolated energy systems, accounting for uncertainty in the renewable generation and the optimal feedback control. To this end, we implement an imitation learning approach to stochastic neural model predictive control (MPC) which allows us to relate the battery storage and wind peak capacities to the emissions reduction and investment costs while accounting for finite horizon, optimal control. Through this approach, decision makers can evaluate the effective emission reduction and costs of different storage and wind capacities at any price point while accounting for uncertainty in the renewable generation with limited foresight. We evaluate the proposed sizing framework on a case study of an offshore energy system with a gas turbine, a wind farm and a battery energy storage system (BESS). In this case, we find a nonlinear, nontrivial relationship between the investment costs and reduction in gas usage relative to the wind and BESS capacities, emphasizing the complexity and importance of accounting for optimal control in the design of isolated energy systems.

**Index Terms**—Model predictive control, imitation learning, stochastic MPC, optimal sizing, isolated energy systems.

## I. INTRODUCTION

Isolated energy systems such as small islands, microgrids, offshore installations, remote communities, or research stations are characterized by their lack of a connection to central grids. In the absence of a base load supply, isolated energy systems often employ in situ fossil gas turbines or diesel generators [33]. Increased attention is paid to decarbonizing isolated energy systems, both to reduce the CO<sub>2</sub> emissions in itself but also due to the often high fuel cost of diesel in remote areas. With the phasing-in of renewable intermittent power sources such as photovoltaic cells and wind turbines, sufficient balancing capacity is needed – yet often obtained by combining energy storage and remaining balancing fossil-fueled backup

sources [35]. In this paper, we address the problem of cost-effective sizing of these hybrid fossil-renewable systems while accounting for the impact of optimal, feedback control of the uncertain renewable power sources during operation. This problem is nontrivial as it involves integrating finite-horizon, stochastic control into a sizing problem of multiple technologies with possible nonlinear cost functions. However, the impact of the control policy including how weather forecasts are integrated and how the uncertain generation is handled may impact the system performance, thus motivating investigation of simplified, combined sizing and control approaches.

Fixed costs or economies-of-scale effects in the investments together with generation uncertainty from the intermittent renewable energy sources cause the sizing of isolated, hybrid-renewable energy systems to be a stochastic, mixed-integer optimization problem. Common approaches to solve this class of problems include two-stage or multi-stage stochastic programming [5] with Benders decomposition to reduce solution times [1], and bi-level optimization [28]. Other approaches include pattern search-based optimization methods with Monte Carlo simulations [6] and frequency-analysis approaches [24]. The first class of methods enables accounting for the uncertainty in renewable generation during the optimal system sizing. Yet, they normally assume perfect, possibly long-term foresight of the renewable generation and thereby fail to account for the effects of a finite prediction horizon, and feedback control, during the actual system operations. Frequency and sampling-based approaches account for the stochasticity and multiple scenarios of weather-dependent renewable generation, while neither account for the multi-variable control of the integrated renewable and energy storage system. Some contributions have been made to account for control in the design of microgrids, e.g. [35], however without rigorously addressing the stochastic control of the intermittent renewable sources. The small size and intermittent nature of the available renewable power sources often in isolated energy systems present new challenges in control and operations. This increase in complexity affects the planning stages of emissions reduction projects as assessing the impact of investment decisions on renewable power and energy storage requires accurate simulations of the system interactions and their optimal operations.

The increase in complexity is commonly dealt with by applying a more advanced control policy such as *model predictive control* (MPC) in which we solve a mathematical dynamic optimization problem at each time step to determine the optimal next action. This has been done in the integration of different energy systems [34], control of an offshore energy system [15], building energy control [13], and microgrid optimization [16], among others. The usage data from the

<sup>1</sup>SINTEF Energy Research, Trondheim, Norway.

This publication has been produced with support from the LowEmission Research Centre ([www.lowemission.no](http://www.lowemission.no)), performed under the Norwegian research program PETROSENTER. The authors acknowledge the industry partners in LowEmission for their contributions and the Research Council of Norway (296207).

control policy can then be used to inform the sizing of the associated energy system [27, 31]. Our approach improves on these by sizing renewable capacity, not just battery capacity, and using imitation learning on an MPC policy to improve runtime which simplifies the process of finding the optimal configuration at a fixed investment budget. Neural MPC of an energy system was recently investigated in [20], where a neural network is trained to imitate a mixed-integer MPC but with a considerably simpler network structure, less focus on risk aspects and no associated investigation into sizing. This paper aims to improve on the limitations of these earlier studies, and our contributions may be summarized as follows:

- We develop a general control-aware sizing framework for energy systems consisting of a power consumer, an intermittent stochastic renewable energy source, a dispatchable thermal generator which can provide backup power, and an energy storage system.
- We train a neural network to imitate the optimal MPC policy for a wide class of capacities, enabling us to estimate residual fuel consumption rapidly. This allows energy-system designers to choose storage and renewable capacities using a lookup table under investment budget and emission reduction constraints, removing the need for an advanced search algorithm for optimal sizing.

A flowchart overview of the steps in determining the optimal sizing can be found in Figure 1.

We demonstrate the proposed methodology on a case study on decarbonization of an offshore energy system. There we are able to reduce runtime substantially compared to a standard MPC approach, allowing us to simulate a wide range of scenarios over different capacity combinations to develop a model for emissions reductions based on sizing, and provide investment advice under a prescribed cost model.

The remainder of this paper is organized as follows: In Section II we briefly go over the formulation of model predictive control and its extensions to imitation learning and taking into account uncertain forecasts. Section III details our sizing framework, including our MPC setup, our neural network architecture, the algorithm for accounting for uncertainty and the investment input procedure. In Section IV we apply this framework to a case study and in Section V we offer concluding remarks.

## II. BACKGROUND

### A. Model predictive control

At a high level, MPC controls a dynamical system to minimize an objective function, subject to constraints for what states our system is allowed to take. In MPC, we take a *receding horizon* approach, meaning that we create a new control plan at each time step over a fixed-length time horizon and only implement the first action of the plan at each time step. In this way, we are able to ensure that we properly account for the long-term impact of our actions while simultaneously being able to rapidly respond to external inputs, system-model mismatch and new information entering our time horizon.

Formally, we split the system variables into three parts – the state variables  $x \in X$  which we can affect indirectly, the

action variables  $u \in U$  which we can choose freely and the exogenous variables  $w \in W$  which are external. The system dynamics are modeled by a function  $f : X \times U \times W \rightarrow X$  satisfying

$$x_{k+1} = f(x_k, u_k, w_k),$$

where a subscript  $k$  corresponds to the value of the variables at the  $k$ -th time step. In this way we are able to recursively determine the state at any future time step  $k+L$  given the actions at time  $k, k+1, \dots, k+L-1$ . Generally, each variable is a vector with either real or integer values.

For an MPC system we generally have constraints such as  $X \subsetneq \mathbb{R}^N$  where  $N$  is the number of variables in the state vector. In its most general form, we encode these constraints into two functions  $g, h : X \times U \times W \rightarrow \mathbb{R}$  of the state, action and exogenous variables so that the constraints are satisfied if and only if  $g \leq 0$  and  $h = 0$ . The next critical component of an MPC system is the objective function  $J$  which is defined over a time horizon of  $H$  steps, i.e.,  $J : X^H \times U^H \times W^H \rightarrow \mathbb{R}$ . For notational convenience, we will take a boldface letter to indicate a vector of the next  $H$  time steps, i.e.,  $\mathbf{x}_k = (x_k, x_{k+1}, \dots, x_{k+H-1})$ . The *control policy*  $\pi : X \times W^H \rightarrow U$  which determines the next action we should take is then defined implicitly by solving the minimization problem

$$\begin{aligned} \min_{\mathbf{u}_k} \quad & J(\mathbf{x}_k, \mathbf{u}_k, \mathbf{w}_k) \\ \text{s.t.} \quad & x_{k+1} = f(x_k, u_k, w_k), \\ & g(x_k, u_k, w_k) \leq 0, \\ & h(x_k, u_k, w_k) = 0, \end{aligned} \quad (1)$$

and letting  $\pi(x_k, \mathbf{w}_k)$  be  $u_k$  from the minimizing argument, i.e., the first component of  $\mathbf{u}_k$ .

### B. Neural model predictive control

The minimization problem (1) can be hard to solve, especially when domains are not connected or one or more of  $J$ ,  $f$ ,  $h$ , or  $g$  are nonlinear. One classical way of circumventing this issue is *explicit MPC* [4, 7] where the policy  $\pi$  is formulated as a lookup table. Under some restrictive conditions on the problem (1) (linear constraints, quadratic objective), it can be shown that the optimal control law is composed of polyhedra that partition the feasible domain. By precomputing these polyhedra, we have essentially exchanged computational cost for storage cost and can apply the optimal control policy with minimal inference latency. However, this solution scales poorly with the number of variables and is generally infeasible for larger systems.

A more modern approach to this problem is to train a neural network to approximate a known good control policy. This falls under the umbrella of *neural MPC* [10, 17] and is called *imitation learning* (IL). In IL, we learn to imitate an expert policy  $\pi^*$  by formulating  $\pi$  as a neural network and choosing its weights by minimizing  $\|\pi^* - \pi\|$ . Without additional work, there are no guarantees that the output  $\hat{u} = \pi(x, w)$  can satisfy  $g \leq 0$  and  $h = 0$ . This can be counteracted, e.g., by adding regularizing terms to the objective function based on  $g$  and  $h$  [2] or manually changing the output  $\hat{u}$  by means of a projection

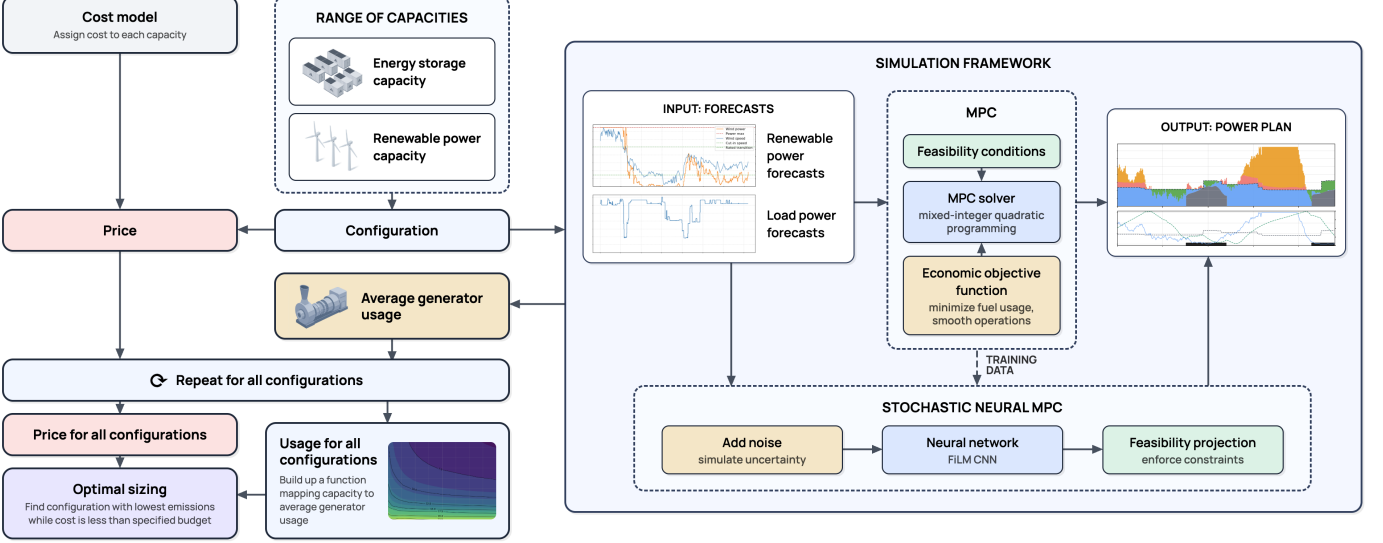


Fig. 1. Overview of the control-aware sizing framework, starting with a cost model and the range of capacities considered and ending in the optimal sizing when generator usage and price for all configurations are known.

$P : \hat{u} \mapsto P(\hat{u}) \in U$  to ensure that the constraints are satisfied [10, 17].

### C. Stochastic model predictive control

So far, we have treated the exogenous variables  $w$  as fixed and determined ahead of time. When this is not the case, it is not clear how one should minimize the objective function  $J$ . This problem is the realm of *stochastic* model predictive control (SMPC) [25]. A common choice to deal with this uncertainty is to consider different scenarios in *scenario-based* or *multi-stage* MPC where we consider branching possibilities for how the system will develop in the future [22]. While popular, this approach suffers from an exponential complexity in the number of time steps to branch over. This can be counteracted by using the output of the scenario-based MPC as the training input to a neural MPC [23] but generating the training data will still suffer from the same increase in complexity and the resulting model will lack interpretability.

In this paper, we detail an alternative approach where we consider a collection of future scenarios, compute the optimal next action for each of them, rank the actions using a metric, and choose based on the quantile. This approach does not require evaluating the objective function in each scenario, meaning that a neural MPC policy can be used. Moreover, different scenarios can be evaluated in parallel, enabling GPU-acceleration. The policy is further detailed in Section III-E.

## III. CONTROL-AWARE SIZING FRAMEWORK

In this section we detail our simulation framework in a general form to highlight its versatility and discuss how it can be applied to sizing. On a high level, we are interested in systems with a conventional power source, the use of which we aim to minimize, a renewable intermittent power source, an energy storage system and a power consumer. We will treat the consumer and the renewable power as external meaning

we cannot affect them and we may not be able to predict them perfectly.

We first introduce the setup of our simulation and the different components before outlining the sizing strategy and describing how the simulation is developed starting from a pure MPC approach and ending with a stochastic neural MPC solution.

### A. System setup and components

Our controller uses a receding horizon approach where the current state and information about the next  $H$  time steps are used to find optimal control actions at the current time step which are applied before moving to the next discrete time step. We let  $T$  denote the total number of time steps in a complete scenario and write  $k$  for the current time step.

We now go over the system components and their characteristic properties. Each component primarily plays a role through its power  $P_k$ .

- **Load  $P_k^{\text{load}}$**  In our energy system, the load comes from the power consumer which has deterministic values for the load at all points in time.
- **Dispatchable thermal generator  $P_k^{\text{DTG}}$**  When renewable power is unavailable, we can use the dispatchable thermal generator to generate power. This system can be turned off and has a minimum power level when online.
- **Energy storage system  $E_k^{\text{ESS}}, P_k^{\text{ESS}}$**  To balance renewable power, we include an energy storage system. Charging and discharging have limited efficiency and the sign of the power will be set so that the power is positive when the ESS is charged and negative when discharged.
- **Renewable power source  $P_k^{\text{RPS}}$**  The future power from the renewable power source will be based on historical data. In our final stochastic approach, we assume that we can sample various possible scenarios for this power source which is relevant in e.g., wind and solar setups

where there exist forecasts for future wind speed and solar irradiance.

The prime goal of the control algorithm is to maintain a power balance where the load power can be met by a combination of the other three components. When the output power is greater than the required power, we need to curtail the excess generation. Formally, we do this by introducing an additional variable  $P_k^{\text{curt}}$ .

### B. Investment input

Our motivation for the control scheme which we will set up is to inform investment decisions on the capacity of the renewable power source and the ESS. Specifically, the performance metric we wish to minimize is the average generator usage as a function of these two capacities

$$G : (E_{\max}^{\text{ESS}}, P_{\max}^{\text{RPS}}) \mapsto P_{\text{avg}}^{\text{DTG}}. \quad (2)$$

The exact interpretations of the capacities  $E_{\max}^{\text{ESS}}$  and  $P_{\max}^{\text{RPS}}$  are made clear in the next section. To estimate this average, we can consider a wide range of load and renewable scenarios and run an MPC for each one of them, averaging the results. Since each simulation runs over  $T$  time steps and depends on the initial state-of-charge, we will choose  $T$  to be large.

Investigating investment decisions requires a cost model. We can represent this as a fully general function  $C$  of  $E_{\max}^{\text{ESS}}$  and  $P_{\max}^{\text{RPS}}$  which can include all of the expenses related to an investment, including the present value of future maintenance and appropriate penalties for using up limited space and weight budgets.

With these two functions in hand, we can make informed investment decisions. Provided that we can sample  $G$  efficiently, it is straightforward to answer questions such as

- (i) Given that the capacities are chosen optimally, what is the average DTG load for each cost?
- (ii) What are optimal energy storage and peak renewable capacities for given budget level or price point, provided that minimum average DTG load is the goal?

These questions can be answered by running a grid search over  $(E_{\max}^{\text{ESS}}, P_{\max}^{\text{RPS}})$ . We will demonstrate this for the case study in Section IV.

### C. Control objective function and constraints

With the convention that the energy storage system power is the derivative of its energy, we can write the total power balance equation as

$$-P_k^{\text{ESS}} + P_k^{\text{DTG}} + P_k^{\text{RPS}} = P_k^{\text{load}} + P_k^{\text{curt}}. \quad (3)$$

Ensuring that the target load is always met is equivalent to only allowing positive curtailment, i.e.,

$$P_k^{\text{curt}} \geq 0. \quad (4)$$

Since the load needs to be met for all time steps, we set the limits for the controllable dispatchable thermal generator high enough that it alone can meet the target load. The fact that the

generator is dispatchable, meaning it can be turned on and off and has a minimum power when online, will be encoded as

$$P_k^{\text{DTG}} \in \{0\} \cup [P_{\min}^{\text{DTG}}, P_{\max}^{\text{DTG}}]. \quad (5)$$

This can be accommodated by means of an auxiliary binary variable which encodes the on/off state at the cost of turning the optimization problem into a mixed-integer problem.

For the energy storage system we utilize an intermediate variable indicating the energy,  $E_k^{\text{ESS}}$ , which is subject to the limits

$$0 \leq E_k^{\text{ESS}} \leq E_{\max}^{\text{ESS}} \quad (6)$$

and the relation

$$E_k^{\text{ESS}} = E_{k-1}^{\text{ESS}} + \Delta t \left( \eta_{\text{ch}} P_{k,+}^{\text{ESS}} - \frac{1}{\eta_{\text{dis}}} P_{k,-}^{\text{ESS}} \right) \quad (7)$$

where  $\eta_{\text{ch}}, \eta_{\text{dis}} \leq 1$  are the charging and discharging efficiencies and  $P_{k,+}^{\text{ESS}}, P_{k,-}^{\text{ESS}} \geq 0$  are the positive and negative parts of  $P_k^{\text{ESS}}$ , respectively. Note that for the  $k=1$  relation, we need an initial condition  $E_0^{\text{ESS}}$ .

Lastly we place limits on the maximum charge/discharge rate of the ESS in the form

$$-P_{\max}^{\text{ESS}} \leq P_k^{\text{ESS}} \leq P_{\max}^{\text{ESS}}. \quad (8)$$

Equations (3) - (8) are all the constraints we will apply.

For our control objective function there will be two terms which promote low and smooth usage of the dispatchable thermal generator;

$$\frac{\lambda_{\text{usage}}^{\text{DTG}}}{H} \sum_{k=1}^H P_k^{\text{DTG}} + \frac{\lambda_{\text{smooth}}^{\text{DTG}}}{H} \sum_{k=1}^H (P_k^{\text{DTG}} - P_{k-1}^{\text{DTG}})^2 \quad (9)$$

where we must manually set a starting value for  $P_0^{\text{DTG}}$ . Note the  $1/H$  factor to make the same coefficients  $\lambda$  work for different time horizons. To minimize degradation of the ESS, we will penalize its usage quadratically. This means that the model will prefer to charge/discharge the battery smoothly. We will also reward the terminal battery level to encourage the model to treat the battery charge as a limited resource throughout the window. These incentives take the form

$$\frac{\lambda_{\text{smooth}}^{\text{ESS}}}{H} \sum_{k=1}^H (P_k^{\text{ESS}})^2 - \lambda_{\text{terminal}}^{\text{ESS}} E_H^{\text{ESS}}. \quad (10)$$

This means that our objective function is

$$J = \frac{\lambda_{\text{usage}}^{\text{DTG}}}{H} \sum_{k=1}^H P_k^{\text{DTG}} + \frac{\lambda_{\text{smooth}}^{\text{DTG}}}{H} \sum_{k=1}^H (P_k^{\text{DTG}} - P_{k-1}^{\text{DTG}})^2 + \frac{\lambda_{\text{smooth}}^{\text{ESS}}}{H} \sum_{k=1}^H (P_k^{\text{ESS}})^2 - \lambda_{\text{terminal}}^{\text{ESS}} E_H^{\text{ESS}}. \quad (11)$$

In total, we can summarize our optimization task as follows: For each time step  $k$ , given  $E_{k-1}^{\text{ESS}}$ ,  $P_{k-1}^{\text{DTG}}$  and sequences  $P_k^{\text{RPS}}$  and  $P_k^{\text{load}}$ , find sequences  $P_k^{\text{DTG}}$  and  $P_k^{\text{ESS}}$  such that (3) - (8) hold, and which minimize (11).

Since the dispatchable thermal generator on/off state needs to be encoded via a binary decision variable, this is a *mixed-integer* optimization problem. Moreover, the objective function

(11) is quadratic in  $P_k^{\text{ESS}}$  and  $P_k^{\text{DTG}}$  and all the constraints are linear. Hence the total problem is a *mixed-integer quadratic programming* (MIQP) problem.

Note that at each time step, we have perfect knowledge with no uncertainty of the current wind which is what affects the power balance up until the next time step. As such, we will always be able to meet the power demand exactly. This simplification is made since we are more interested in the high-level behavior of our system, mostly with respect to the utilization of the dispatchable thermal generator. In a real installation, we would have another controller acting on shorter time scales to smooth out the short-term power variability.

Solving the MIQP problem iteratively with a receding horizon yields a valid MPC policy. While this works fine, the approach suffers from the problems mentioned in Section II. Before dealing with uncertainties in the future load and renewable power, we first improve the runtime of the model by approximating it with a neural network in the next section.

#### D. Imitation learning

The goal of our neural MPC model is to approximate the actual MPC policy detailed above while significantly reducing runtime, similar to the setup in [20]. Since our ultimate goal is to use our control policy to compare the behaviors of our system with different ESS and renewable power capacities, we want to be able to condition the model on this. We do this by choosing a global maximum ESS capacity and renewable power capacity and then always conditioning our model on these two scale parameters during training and inference. To deal with possibly different output ranges based on these scales, we will restrict the model to output in the  $[0, 1]$  range for the dispatchable energy source and the  $[-1, 1]$  range for ESS power and then rescale by  $P_{\max}^{\text{DTG}}$  and  $P_{\max}^{\text{ESS}}$  respectively.

1) *Training data*: Having set up our optimal control problem, we can sample the MPC algorithm at random states to get optimal next actions. Specifically, we want to learn the mapping

$$(E_{k-1}^{\text{ESS}}, P_{k-1}^{\text{DTG}}, P_k^{\text{RPS}}, P_k^{\text{load}}) \mapsto (P_k^{\text{ESS}}, P_k^{\text{DTG}}),$$

conditioned on random renewable and ESS scales in  $[0, 1]$ . We do this by solving the MIQP problem for randomly selected real renewable power and target load scenarios with randomly chosen initial ESS state-of-charge and previous dispatchable thermal generator usage. We only run the solver for one time step before sampling a new scenario to maximize data diversity. This process is highly parallelizable and we run it offline to collect data for the model training.

2) *Model architecture*: To learn the control problem, we train a ResNet-v2-style [14] convolutional neural network (CNN) with GroupNorm, GELU activations, and feature-wise linear modulation (FiLM) [26] to encode the current ESS state-of-charge and DTG usage, as well as the ESS and renewable capacities. The architecture is illustrated in detail in Figure 2. The future load and renewable power are treated as a 2-channel time series which is first mapped to a tensor of shape  $(C, H)$  where  $C$  is the number of hidden channels, by means of a convolutional layer with kernel size 1. The FiLM conditioning

takes the form of two vectors  $\gamma, \beta$ , each of length  $C$ , which are the output of a simple 2-layer MLP, which are applied inside each ResNet block as  $h \mapsto h(1 + \gamma) + \beta$ . After the final block, we take the mean over  $H$  to get a vector of length  $C$  which we connect to an output head which is a 2-layer MLP which outputs two numbers. We finally apply a hyperbolic tangent to one of the outputs and a sigmoid mapping to the other and these are  $\widehat{P_k^{\text{ESS}}}$  and  $\widehat{P_k^{\text{DTG}}}$  respectively. The hyperbolic tangent and sigmoid allow us to properly account for their power limits (8) and (5).

3) *Action projection*: As discussed in Section II-B, since the neural network output does not exactly match the deterministic MPC algorithm, there is no guarantee that the actions it recommends are valid in the sense of conforming to the constraints (3) - (8). To solve this problem, we apply light post-processing of the outputs  $\widehat{P_k^{\text{DTG}}}, \widehat{P_k^{\text{ESS}}}$  to ensure that the constraints hold. We refer to this processing as a projection since it maps to the space of valid actions and is the identity on that space.

The most important constraint is the power balance equation (3). Since negative curtailment is not allowed, in the case that

$$P_k^{\text{RPS}} + \widehat{P_k^{\text{DTG}}} - \widehat{P_k^{\text{ESS}}} < P_k^{\text{load}}$$

we need to increase  $\widehat{P_k^{\text{DTG}}}$  or decrease  $\widehat{P_k^{\text{ESS}}}$  while still adhering to (3) - (8). We can do this by dispatching power from the ESS with contingencies for using the thermal generator or both depending on the power and energy limits. Similarly, to ensure that (5) holds, we map network outputs for the dispatchable thermal generator power in  $[0, P_{\min}^{\text{DTG}}/2)$  to 0 and outputs in  $[P_{\min}^{\text{DTG}}/2, P_{\min}^{\text{DTG}})$  to  $P_{\min}^{\text{DTG}}$ .

On top of ensuring that all the constraints hold, we can further increase the performance of the neural MPC solution by explicitly forbidding simultaneous battery discharge and curtailment since this will never be the case in any solution of (1). We view these corrective actions as the final step of the neural MPC so that going forward we can safely assume that anything the neural MPC algorithm outputs is a valid action.

#### E. Scenario handling of uncertainties

Having set up our neural MPC model which can run fast inference, we turn to using it as part of a custom stochastic MPC algorithm. Specifically, given that the neural MPC inference is quick and only returns the next optimal action, we propose the following stochastic MPC algorithm based on an economic robustness metric  $r : U \rightarrow \mathbb{R}$  and a parameter  $\alpha \in [0, 1]$ :

- 1) Sample  $N$  different future scenarios via their corresponding exogenous variables  $\{\mathbf{w}_k^n\}_{n=1}^N$ .
- 2) Compute the next action recommended by  $\pi$  for each scenario as

$$\mathcal{A}_N = \{\pi(x_k, \mathbf{w}_k^n)\}_{n=1}^N.$$

- 3) Sort the actions  $\mathcal{A}_N$  based on the economic robustness metric  $r$ .
- 4) Choose an action at the  $\alpha$ -quantile in the sorted list.

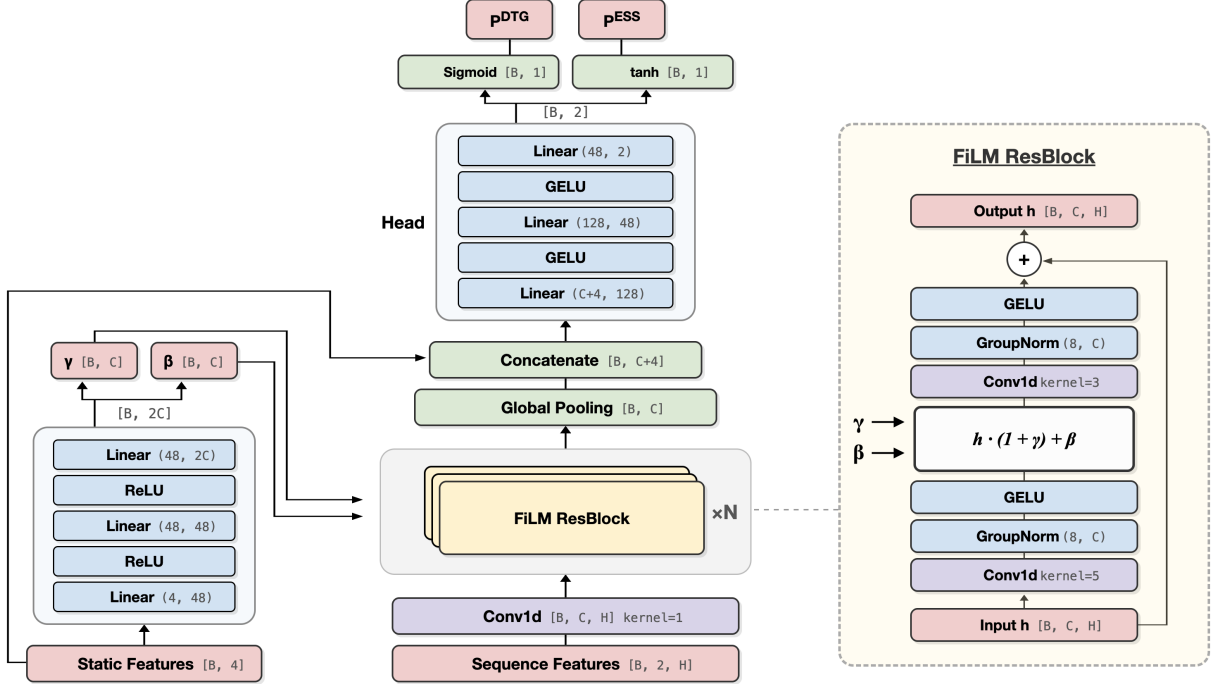


Fig. 2. Overview of the architecture of the network used in the neural MPC. The parameters  $B, C, H$  are the batch size, number of hidden channels and sequence length respectively.

*Remark.* Step 2 can be done in parallel, and if  $\pi$  is a neural MPC policy we can stack the scenarios along the batch dimension, increasing performance substantially.

Note in particular that the economic robustness metric is a function of a single action. Since we are never at risk of not being able to meet the power demand, our notion of economic robustness is related to minimizing the risk of running out of stored energy and having to ramp up the DTG rapidly due to unexpected future low renewable production. To hedge against this scenario, we should run the DTG in the near term and charge the ESS. As such, we choose

$$r(P^{\text{DTG}}, P^{\text{ESS}}) = P^{\text{DTG}} + P^{\text{ESS}}. \quad (12)$$

One interpretation of this formula is that it is the “safe” power which we activate to be in a better position in the future.

As an illustrative example, consider the case where there is a 10 MW power deficiency after accounting for the renewable power which needs to be met by the dispatchable thermal generator and/or discharging the ESS. If we are risk-averse, we would not want to discharge the ESS and instead run the DTG. Both of these choices contribute to increasing the value of  $r$ . Similarly, in the case where renewable power is greater than the load target, we will most likely not run the DTG at all and instead charge the ESS. If we are risk-averse, we might opt to charge the ESS over a shorter time horizon, since we are unsure if the strong winds will stay, meaning that  $P_k^{\text{ESS}}$  will be higher which corresponds to a higher value of  $r$  again.

Under the assumption that the proposed scenarios accurately reflect the future, this algorithm allows us to properly account for our risk appetite via the parameter  $\alpha$  where a higher value of  $\alpha$  means that we adopt a policy which is more

economically robust. While this is a general and easy-to-implement approach, we did have to define our own function  $r$ . However, the case can be made that defining the risk through an explicit economic robustness metric rather than implicitly through the objective function is preferable since the objective function is formulated to describe the optimal action in a single scenario, not relative notions such as “take the action which is more risk-averse than needed in 90% of plausible scenarios”.

*Remark.* Related ideas for stochastic MPC can be found in the literature under names including *multi-forecast* MPC [29] and *multi-scenario* MPC [32]. However, to the best of our knowledge, the setup as described here of computing entirely separate optimal next actions for a collection of scenarios and then choosing one based on some ranking has not previously been investigated. In particular, the amenability of neural MPC algorithms with batching to this problem has not been discussed elsewhere either to the best of our knowledge.

#### IV. CASE STUDY: DECARBONIZING AN OFFSHORE ENERGY SYSTEM

In this case study we consider a hypothetical offshore energy system on the Norwegian continental shelf (NCS), where the goal is to decarbonize the energy generation. The system is powered by wind turbines, with a single gas turbine for backup, and a battery energy storage system (BESS).

##### A. System overview

We first give an overview of the power producers and consumers on the platform.

- **Load source  $P_k^{\text{load}}$**  We have access to proprietary energy usage data from a platform on the NCS provided by one

of the operators in the LowEmission centre [21]. This data is sampled at  $\Delta t = 1$  h but we can sub- or super-sample it to align with the  $\Delta t$  of the renewable power source. A subset of the load data is displayed in Figure 3. As we see in the figure, the nominal power consumption is around 30 MW.

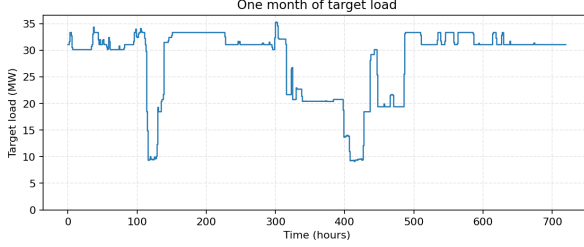


Fig. 3. Example of the target load data over a month.

- **Dispatchable thermal generator  $P_k^{\text{GT}}$**  The dispatchable thermal generator for our system is a single gas turbine. We set  $P_{\max}^{\text{GT}} = 40$  MW and  $P_{\min}^{\text{GT}} = 0.35 \cdot 40$  MW to roughly match a conventional offshore gas turbine [30]. Rapid ramping of the gas turbine is discouraged by the smoothness term in the objective function.
- **Energy storage system  $E_k^{\text{BESS}}$ ,  $P_k^{\text{BESS}}$**  A realistic form of energy storage system for an offshore energy system platform is a battery energy storage system (BESS). We set  $\eta_{\text{ch}} = \eta_{\text{dis}} = 0.96$  for a roughly 92% roundtrip efficiency which is consistent with industry numbers for Li-ion batteries [18]. We choose a  $C$ -rate of 1 hour which means that  $P_{\max}^{\text{BESS}} = \frac{E_{\max}^{\text{BESS}}}{1 \text{ h}}$ .
- **Renewable power source  $P_k^{\text{WTG}}$**  We use a wind turbine generator (WTG) as our renewable power source and its interaction with the complete system is purely as an exogenous signal. As a data source we use wind speed observations from 2020 at the Brage offshore platform [11]. The wind data can then be converted to power via the cubic relation  $P_k^{\text{WTG}}(v) = A_3 v^3 + A_2 v^2 + A_1 v + A_0$  with constants from [12] for wind speeds above a set cut-in speed, as a constant  $P_{\max}^{\text{WTG}}$  above the rated wind speed, and as 0 below the cut-in or above the cut-out speed. A subset of the wind speed data and the associated wind power data is shown in Figure 4. The sampling interval

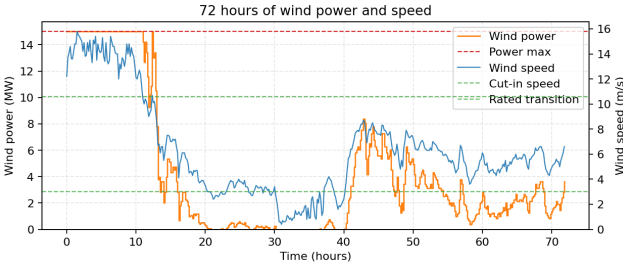


Fig. 4. Example of wind speed and power data over a three-day period.

of the data is  $\Delta t = 10$  min so we use this for all of our time series.

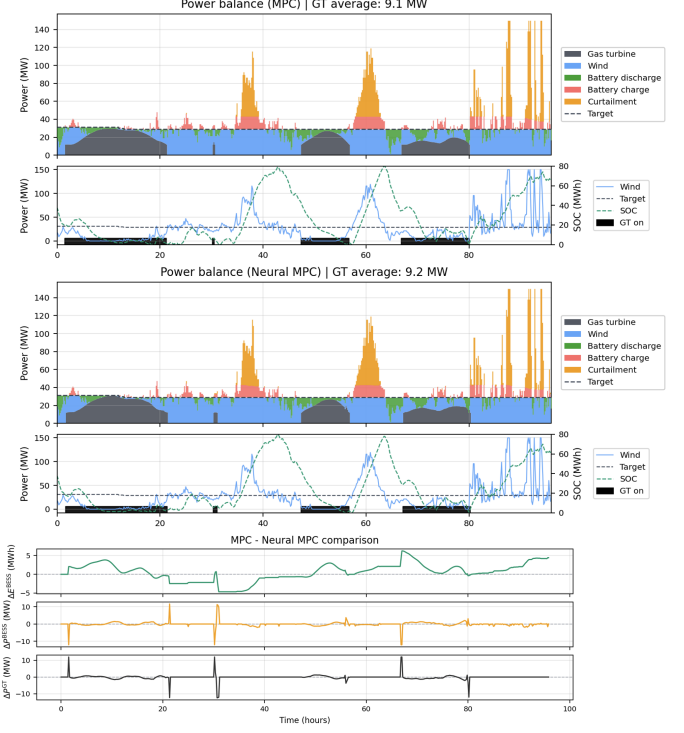


Fig. 5. Power plans for standard MPC (top) and neural MPC (middle) for the same scenario. The bottom subfigure highlights the discrepancies in BESS energy, power and gas turbine power between standard and neural MPC.

## B. MPC results

In this section we discuss the actual MPC algorithm applied to the energy system of the case study.

1) *Deterministic MPC*: Through trial-and-error, we have found that the following parameter values perform well for the deterministic MPC algorithm.

$$\begin{aligned} \lambda_{\text{usage}}^{\text{GT}} &= 1, & \lambda_{\text{smooth}}^{\text{BESS}} &= 2 \cdot 10^{-3}, \\ \lambda_{\text{smooth}}^{\text{GT}} &= 0.6, & \lambda_{\text{terminal}}^{\text{BESS}} &= 10^{-2}. \end{aligned}$$

We have also chosen a look-ahead window of 6 hours which corresponds to  $H = \frac{6 \text{ h}}{\Delta t} = 36$  time steps. For the examples in this section we set  $P_{\max}^{\text{WTG}} = 150$  MW and  $E_{\max}^{\text{BESS}} = 80$  MWh which is large enough that we see large amounts of interaction between the different system components.

The MIQP problem is solved using the *Solving Constraint Integer Programs* (SCIP) solver [9]. In the top subfigure in Figure 5 we see the result of the MPC control policy for a selected scenario. In that figure, we see the effect of the objective function in the smooth ramping of the gas turbine, the discharging of the battery around hour 45 to delay starting the gas turbine, and the even charging rate leading to full charge during periods of high wind.

2) *Neural MPC*: To train our neural MPC algorithm, we sample 600 000 actions from the MPC algorithm specified above with input data chosen randomly as specified in Section III-D1. For the model described in Section III-D2, we choose a hidden channel dimension of 96, 4 blocks, hidden conditioning dimension 48, and a head with hidden dimensions (128, 48), resulting in a relatively small model with a total of 327,954

parameters. These values were selected by means of a brief hyperparameter search performed using Optuna [3].

We train with Huber loss for 50 epochs with the AdamW optimizer, a batch size of 512 and a learning rate of  $4 \cdot 10^{-4}$ . This leads to a validation Huber loss of 0.14 and a mean absolute error (MAE) of 0.29 MW. Note however that due to the discontinuous nature of gas turbine usage, we should expect the errors to be extremely heavy-tailed which is why we opt for Huber loss over mean squared error. See the bottom part of Figure 5 for an example of how the errors look in a full rollout. LSTM- and transformer-based methods were also considered and found to perform worse than the CNN.

The neural MPC model generally performs very similarly to the deterministic MPC, especially after the action projection described in Section III-D3. This can be seen by comparing the two action sequences in Figure 5. In the bottom subfigure, we see the exact differences which are generally concentrated to the exact time step during which the gas turbine is started and stopped. Note also that the average gas turbine usage (9.1 MW and 9.2 MW) are very close which is the metric which is important for sizing decisions.

The neural MPC algorithm runs through a 4-day period of  $T = 960$  time steps in around 4 seconds on a MacBook Pro M2, compared to around 2 minutes for the standard MPC algorithm which in addition has a high variability in runtime.

3) *Stochastic neural MPC*: We model uncertainty in the renewable generation via a collection of scenarios for the future, each equally likely. To generate these scenarios, we take the historical wind speed for the next  $H$  time steps, add a random walk with standard deviation 0.5 m/s and clip the resulting wind speed at zero. We then compute wind power using the cubic relation described in Section IV-A. This means that if the wind speed is far below the wind turbine cut-in, different scenarios may not change the wind power, which is not uncommon.

In implementing the algorithm described in Section III-E, we choose  $\alpha = 0.6$  to err slightly on the risk-averse side and  $N = 64$  scenarios. The resulting average gas turbine utilization over a collection of scenarios for different values of  $\alpha$  is illustrated in Figure 6. Here we see that choosing a high quantile meaning being more pessimistic about future wind power, generally leads to higher gas turbine usage. Similarly, being overly optimistic also leads to increased gas turbine usage. The choice  $\alpha = 0.5$ , corresponding to the median action with respect to our robustness metric leads to the lowest average gas turbine usage with this specific scenario-generation procedure.

In Figure 7, the considered wind scenarios and the associated actions as given by the neural MPC algorithm are visualized as histograms and a scatter plot with the actions in the  $\alpha$ -quantile selected with respect to (12) highlighted in red.

In the top half of the figure, we see all the considered wind scenarios as well as the historical data they are based on, all starting from the current wind speed. It is the top row, i.e., the current gas turbine usage, battery state-of-charge and future wind profile, as well as the future target load which is the input to the neural network.

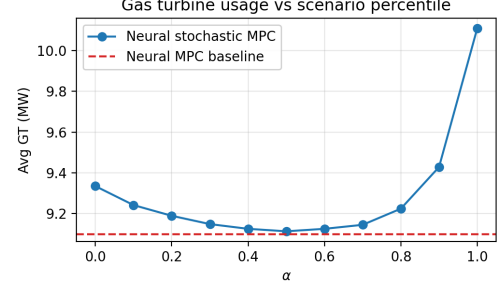


Fig. 6. Gas turbine usage as a function of the risk parameter  $\alpha$ . The dashed red line indicates the neural MPC with exact forecast as input.

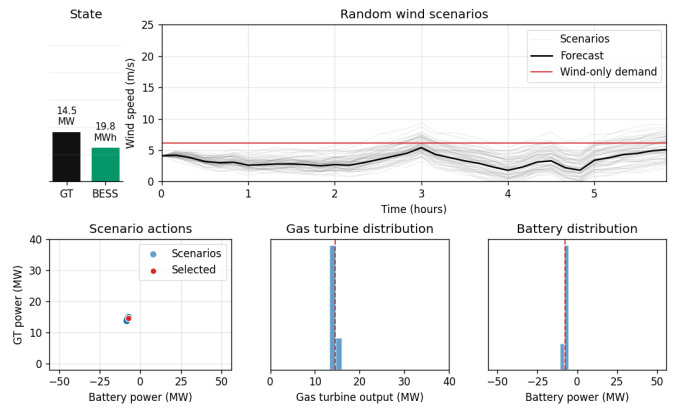


Fig. 7. Snapshot of a single time step for the neural stochastic MPC process and its view of the time horizon. In the top row is the current state and the collection of possible wind scenarios based on the forecast, together with the red line indicating the wind speed required to power the platform completely by wind. In the bottom row is a scatter plot as well as histograms of the suggested gas turbine and battery powers for the different scenarios.

### C. Sizing results

Recall that we trained all our algorithms to handle different sized BESS units and wind farms. In Figure 8, we compare the same scenario with BESS capacities of 8 MWh and 80 MWh. There we see that with the larger battery we are able to avoid turning on the gas turbine in three out of the four time periods with low wind and thereby decreasing the average gas turbine usage from 9.6 MW to 3.1 MW.

For the investment costs, we use an affine cost function with marginal and fixed costs given by

$$C(E_{\max}^{\text{BESS}}, P_{\max}^{\text{WTG}}) = A_{\text{BESS}} E_{\max}^{\text{BESS}} + B_{\text{BESS}} + A_{\text{WTG}} P_{\max}^{\text{WTG}} + B_{\text{WTG}}.$$

Using rough estimates based on publicly available data [8, 19] while accounting for additional costs due to offshore deployment, we set  $A_{\text{WTG}} = 5 \text{ M€/MW}$ ,  $B_{\text{WTG}} = 35 \text{ M€}$  and  $A_{\text{BESS}} = 0.6 \text{ M€/MWh}$ ,  $B_{\text{BESS}} = 20 \text{ M€}$ . We remark that these numbers are illustrative and may not capture the complete, location-dependent costs of offshore installations. Applying the proposed imitation learning methodology in Section III-D, running extensive simulations like those in Figure 8 for different wind and BESS capacities, we estimate the average gas turbine usage (2) and relative investment costs

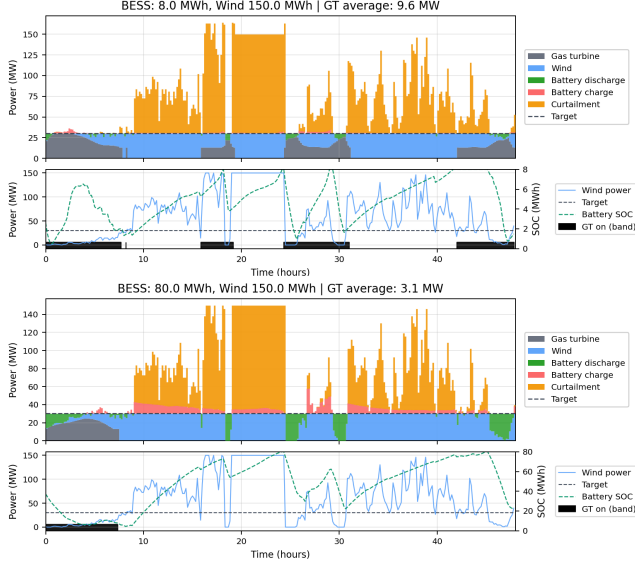


Fig. 8. The same wind and load scenario simulated with an 8 MWh and an 80 MWh battery.

as shown in the left of Figure 9. For each combination of these wind and BESS capacities, we find the corresponding investment costs and average gas turbine usage illustrated to the right in Figure 9.

In the left of Figure 9 we see that the very lowest investments have limited effects on the emissions reductions which is due to the fixed cost of wind power. Specifically, the model can initially only utilize the BESS which can be seen from the horizontal red line in the bottom left corner of the right subfigure. Once the budget is enough to accommodate the fixed cost of wind power, we see a rapid decline in emissions up to around 250 M€ after which the effect tapers off, indicating that this could be an efficient investment level. In the right subfigure, the labels indicate cost in millions of euros, starting at the bottom left corner. In this particular example, the optimal investment path is to add wind turbines up to the nominal platform load and then scale up batteries together with wind capacity. Note that BESS capacity becomes saturated at the 80 MWh limit around 350 M€.

In a real scenario, one would most likely use a non-affine cost model to account for the limited weight and space on an offshore platform. Still, the high-level insights from this analysis are likely to remain relevant. We have seen that a mixture of wind and batteries can be cost competitive with a purely wind-based approach and as batteries continue to drop in price and increase in density, this conclusion should grow even more compelling.

## V. CONCLUDING REMARKS

We set up a framework for the optimal sizing of isolated energy systems which uses accurate estimates of the fuel consumption for a wide class of systems by learning an MPC policy and running it for a collection of scenarios. This framework was then applied in a case study enabling decision makers to identify optimal investment capacities for wind and BESS given a budget level. A direct output of the framework

is the expected emission reduction, by means of resulting average gas turbine usage, accounting for a large set of weather scenarios and stochastic MPC system operations.

The implemented sizing methodology applies an exhaustive exploration of the decision space for obtaining an explicit map of expected generator usage and investment costs. The problem described in Section III-B can be formally treated as a multi-objective optimization problem, to which for instance direct search algorithms can be applied for systems with more technologies to be evaluated for the investments.

The imitation learning method for the stochastic neural MPC model discussed in the paper has the potential to be utilized for analysis of other systems and control problems, while the sizing framework is applicable for many types of isolated energy systems including systems with both PV and wind energy, mixed storages, and diesel instead of gas turbines for backup. Our architecture and setup for imitation learning neural MPC are formulated in a general way and are likely to be useful for future work in the field.

## ACKNOWLEDGMENTS

The authors thank Saket Adhau for insightful discussions during the early stages of this work.

## REFERENCES

- [1] M. A. Abdulgalil and S. Member, "Optimizing a distributed wind-storage system under critical uncertainties using Benders decomposition," *IEEE Access*, vol. 7, pp. 77951–77963, 2019. DOI: 10.1109/ACCESS.2019.2922619
- [2] S. Adhau, V. V. Naik, and S. Skogestad, "Constrained Neural Networks for Approximate Nonlinear Model Predictive Control," in *2021 60th IEEE Conference on Decision and Control (CDC)*, IEEE, 2021, pp. 295–300. DOI: 10.1109/cdc45484.2021.9683320
- [3] T. Akiba, S. Sano, T. Yanase, T. Ohta, and M. Koyama, "Optuna: A Next-Generation Hyperparameter Optimization Framework," in *The 25th ACM SIGKDD International Conference on Knowledge Discovery & Data Mining*, 2019, pp. 2623–2631. DOI: 10.1145/3292500.3330701
- [4] A. Alessio and A. Bemporad, "A Survey on Explicit Model Predictive Control," in *Nonlinear Model Predictive Control*. Springer Berlin Heidelberg, 2009, pp. 345–369. DOI: 10.1007/978-3-642-01094-1\_29
- [5] H. Alharbi, A. Indices, and B. Parameters, "Stochastic Optimal Planning of Battery Energy Storage Systems for Isolated Microgrids," *IEEE Trans. Sustain. Energy*, vol. 9, no. 1, pp. 211–227, 2018. DOI: 10.1109/TSTE.2017.2724514
- [6] A. Arabali, M. Ghofrani, M. Etezadi-Amoli, and M. S. Fadali, "Stochastic performance assessment and sizing for a hybrid power system of Solar/Wind/Energy Storage," *IEEE Trans. Sustain. Energy*, vol. 5, no. 2, pp. 363–371, 2014. DOI: 10.1109/TSTE.2013.2288083
- [7] A. Bemporad, M. Morari, V. Dua, and E. N. Pistikopoulos, "The explicit linear quadratic regulator for constrained systems," *Automatica*, vol. 38, no. 1, pp. 3–20, 2002. DOI: 10.1016/s0005-1098(01)00174-1
- [8] BloombergNEF, *Battery storage system cost survey 2024 (turnkey system prices)*, Reported in e.g. "BNEF finds 40 % year-on-year drop in BESS costs", 2024. [Online]. Available: <https://www.energy-storage.news/behind-the-numbers-bnef-finds-40-year-on-year-drop-in-bess-costs/>
- [9] S. Bolusani et al., "The SCIP Optimization Suite 9.0," *Optimization Online*, 2024. [Online]. Available: <https://www.scipopt.org/>

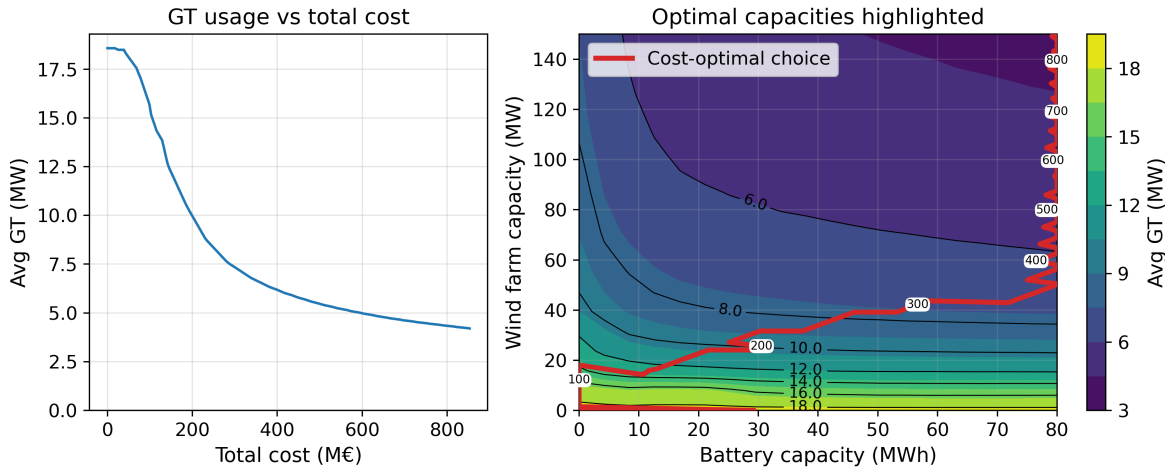


Fig. 9. Optimal investment and results for a given cost model for wind and BESS capacity. Left: Average gas turbine usage as a function of total investment in wind and BESS with cost-optimal choices. Right: Contour plot of average gas turbine usage as a function of battery and wind capacity. Overlaid in red is the optimal investments at different price points, with multiples of 100 M€ highlighted.

- [10] S. Chen et al., "Approximating Explicit Model Predictive Control Using Constrained Neural Networks," in *2018 Annual American Control Conference (ACC)*, IEEE, 2018. DOI: 10.23919/acc.2018.8431275
- [11] *Frost API*, <https://frost.met.no/index.html>, Accessed: 2025-09-30, MET Norway.
- [12] E. Gaertner et al., "Definition of the IEA 15-megawatt offshore reference wind turbine," International Energy Agency, Tech. Rep., 2020. [Online]. Available: <https://www.nrel.gov/docs/fy20osti/75698.pdf>
- [13] Y. Gao, Y. Matsunami, S. Miyata, and Y. Akashi, "Model predictive control of a building renewable energy system based on a long short-term hybrid model," *Sustainable Cities and Society*, vol. 89, p. 104317, 2023. DOI: 10.1016/j.scs.2022.104317
- [14] K. He, X. Zhang, S. Ren, and J. Sun, "Identity Mappings in Deep Residual Networks," in *Proceedings of the European Conference on Computer Vision (ECCV)*, Springer, 2016, pp. 630–645. DOI: 10.1007/978-3-319-46493-0\_38
- [15] K. T. Hoang, C. A. Thilker, B. R. Knudsen, and L. S. Imsland, "A hierarchical framework for minimising emissions in hybrid gas-renewable energy systems under forecast uncertainty," *Applied Energy*, vol. 373, p. 123796, 2024. DOI: 10.1016/j.apenergy.2024.123796
- [16] J. Hu et al., "Economic Model Predictive Control for Microgrid Optimization: A Review," *IEEE Transactions on Smart Grid*, vol. 15, no. 1, pp. 472–484, 2024. DOI: 10.1109/tsg.2023.3266253
- [17] B. Karg and S. Lucia, "Efficient Representation and Approximation of Model Predictive Control Laws via Deep Learning," *IEEE Transactions on Cybernetics*, vol. 50, no. 9, pp. 3866–3878, 2020. DOI: 10.1109/tcyb.2020.2999556
- [18] A. A. Kebede, T. Kalogiannis, J. Van Mierlo, and M. Bercicbar, "A comprehensive review of stationary energy storage devices for large scale renewable energy sources grid integration," *Renewable and Sustainable Energy Reviews*, vol. 159, p. 112213, 2022. DOI: 10.1016/j.rser.2022.112213
- [19] N. R. E. Laboratory, "Cost of Wind Energy Review: 2024 Edition," NREL, Tech. Rep. NREL/PR-5000-91775, 2024. [Online]. Available: <https://docs.nrel.gov/docs/fy25osti/91775.pdf>
- [20] C. Liu, S. Shi, A. Alan, G. K. Venayagamoorthy, and B. D. Schutter, *Approximate Model Predictive Control for Microgrid Energy Management via Imitation Learning*, 2025. arXiv: 2510.20040 [eess.SY].
- [21] LowEmission, *LowEmission – Reducing emissions on the Norwegian continental shelf*, <https://www.lowemission.no/>.
- [22] S. Lucia, T. Finkler, and S. Engell, "Multi-stage nonlinear model predictive control applied to a semi-batch polymerization reactor under uncertainty," *Journal of Process Control*, vol. 23, no. 9, pp. 1306–1319, 2013. DOI: 10.1016/j.jprocont.2013.08.008
- [23] S. Lucia and B. Karg, "A deep learning-based approach to robust nonlinear model predictive control," *IFAC-PapersOnLine*, vol. 51, no. 20, pp. 511–516, 2018. DOI: 10.1016/j.ifacol.2018.11.038
- [24] Y. V. Makarov, P. Du, M. C. Kintner-Meyer, C. Jin, and H. F. Illian, "Sizing Energy Storage to Accommodate High Penetration of Variable Energy Resources," *IEEE Trans. Sustain. Energy*, vol. 3, no. 1, pp. 34–40, 2012. DOI: 10.1109/TSTE.2011.2164101
- [25] A. Mesbah, "Stochastic Model Predictive Control: An Overview and Perspectives for Future Research," *IEEE Control Systems*, vol. 36, no. 6, pp. 30–44, 2016. DOI: 10.1109/mcs.2016.2602087
- [26] E. Perez, F. Strub, H. de Vries, V. Dumoulin, and A. Courville, "FiLM: Visual Reasoning with a General Conditioning Layer," *Proceedings of the AAAI Conference on Artificial Intelligence*, vol. 32, no. 1, 2018. DOI: 10.1609/aaai.v32i1.11671
- [27] A. Al-Quraan and B. Al-Mhairat, "Economic predictive control-based sizing and energy management for grid-connected hybrid renewable energy systems," *Energy*, vol. 302, p. 131795, 2024. DOI: 10.1016/j.energy.2024.131795
- [28] R. Rigo-mariani, B. Sareni, and X. Roboam, "Integrated optimal design of a smart microgrid with storage," *IEEE Trans. Smart Grid*, vol. 8, no. 4, pp. 1762–1770, 2017. DOI: 10.1109/TSG.2015.2507131
- [29] X. Shen and S. Boyd, "Incremental Proximal Multi-Forecast Model Predictive Control," arXiv: 2111.14728 [math.OC].
- [30] Siemens, *SGT-750 Gas Turbines – Technical Data*, Accessed: 2025-10-28, 2023. [Online]. Available: <https://www.siemens-energy.com/global/en/home/products-services/product/sgt-750.html>
- [31] Z. Su, Y. Ju, Z. Wang, and S. Moura, "Optimal battery sizing model sensitive to control strategies in microgrids," in *Proceedings of Building Simulation 2023: 18th Conference of IBPSA*, ser. BS 2023, vol. 18, IBPSA, 2023. DOI: 10.26868/2522708.2023.1495
- [32] X. Tian, Y. Guo, R. R. Negenborn, L. Wei, N. M. Lin, and J. M. Maestre, "Multi-Scenario Model Predictive Control Based on Genetic Algorithms for Level Regulation of Open

Water Systems under Ensemble Forecasts," *Water Resources Management*, vol. 33, no. 9, pp. 3025–3040, 2019. DOI: 10.1007/s11269-019-02284-x

[33] R. D. Trevizan, A. J. Headley, R. Geer, S. Atcity, and I. Gyuk, "Integration of energy storage with diesel generation in remote communities," *MRS Energy & Sustainability*, vol. 8, no. 2, pp. 57–74, 2021. DOI: 10.1557/s43581-021-00013-9

[34] A. Turk, Q. Wu, and M. Zhang, "Model predictive control based real-time scheduling for balancing multiple uncertainties in integrated energy system with power-to-x," *International Journal of Electrical Power & Energy Systems*, vol. 130, p. 107015, 2021. doi: 10.1016/j.ijepes.2021.107015

[35] A. Zhou, S. Member, R. Yan, and T. K. Saha, "Capacity and Control Strategy Design of Isolated Micro-Grid With High Renewable Penetration," *IEEE Trans. Sustain. Energy*, vol. 11, no. 3, pp. 1173–1184, 2020. DOI: 10.1109/TSTE.2019.2920274